Disorder in pentachloronitrobenzene, $C_6Cl_5NO_2$: a diffuse scattering study

Lynne H. Thomas,[a] T. Richard Welberry,[b]* Darren J. Goossens,[b] Aidan P. Heerdegen,[b] Matthias J. Gutmann,[c] Simon J. Teat,[d] Peter L. Lee,[e] Chick C. Wilson[f] and Jacqueline M. Cole[a,g]*

[a]University Chemical Laboratory, University of Cambridge, Lensfield Road, Cambridge CB2 1EW, England, [b]Research School of Chemistry, Australian National University, Canberra, ACT 0200, Australia, [c]ISIS Facility, Rutherford Appleton Laboratory, Chilton, Didcot, Oxon OX11 0QX, England, [d]Synchrotron Radiation Department, Daresbury Laboratory, Warrington WA4 4AD, England, [e]Advanced Photon Source, Argonne National Laboratory, Argonne, Illinois, USA, [f]Department of Chemistry and WestCHEM Research School, University of Glasgow, Glasgow G12 8QQ, Scotland, and [g]Cavendish Laboratory, University of Cambridge, J. J. Thomson Avenue, Cambridge CB3 0HE, England

Correspondence e-mail:
welberry@rsc.anu.edu.au,
jmc61@hermes.cam.ac.uk

Monte Carlo computer simulation has been used to interpret and model observed single-crystal diffuse X-ray scattering data for pentachloronitrobenzene, $C_6Cl_5NO_2$. Each site in the crystal contains a molecule in one of six different basic orientations with equal probability. However, no short-range order amongst these different orientations has been detected. The strong, detailed and very distinctive diffraction patterns can be accounted for almost entirely on the assumption of random occupancy of each molecular site, but with very large local relaxation displacements that tend to increase the neighbouring distances for contacts involving $NO_2 \cdots NO_2$ and $NO_2 \cdots Cl$ with a corresponding reduction for those involving $Cl \cdots Cl$. The results show that the mean $NO_2 \cdots NO_2$ distance is increased by ~ 0.6 Å, compared with that given by the average structure determination.

1. Introduction

Although the average crystal structure of materials (as revealed by conventional Bragg scattering crystallography) may go some way towards providing an understanding of their physical properties, it is clear that for many technologically important materials this is quite insufficient and that their special and sometimes exceptional properties are intimately associated with the disorder or short-range order in them, *i.e.* their nanoscale structure. Examples include substitutional disorder in superconductors and shape-memory devices, formation of polar nanodomains in relaxor ferroelectrics, orientational disorder in liquid crystals and dynamic disorder in cyclopentadienyl rings in organometallic contenders for polymerization catalysts. Despite the evident importance of disorder, however, it is often quantified indirectly either by spectroscopic methods (*e.g.* NMR or inelastic neutron scattering) or by inferring models of the disorder from the results of conventional Bragg structural analysis. However, this need not be the case: the diffraction patterns of a disordered material are often rich in additional structural information (both static and dynamic), in the form of structured diffuse scattering. If captured and analysed suitably, in tandem with Bragg measurements, the level of direct information obtainable from diffraction can far supersede that available from indirect spectroscopic methods. The combined use of Bragg and diffuse scattering, the so-called total scattering, of a diffraction pattern to interpret disorder is highly desirable and it is this method we have used in the work presented here. The recording and analysis of diffuse scattering from all kinds of different materials has developed considerably in recent years (Welberry, 2004). In this paper we use these methods to investigate the disorder in pentachloronitrobenzene, $C_6Cl_5NO_2$, hereafter referred to as PCNB.

research papers

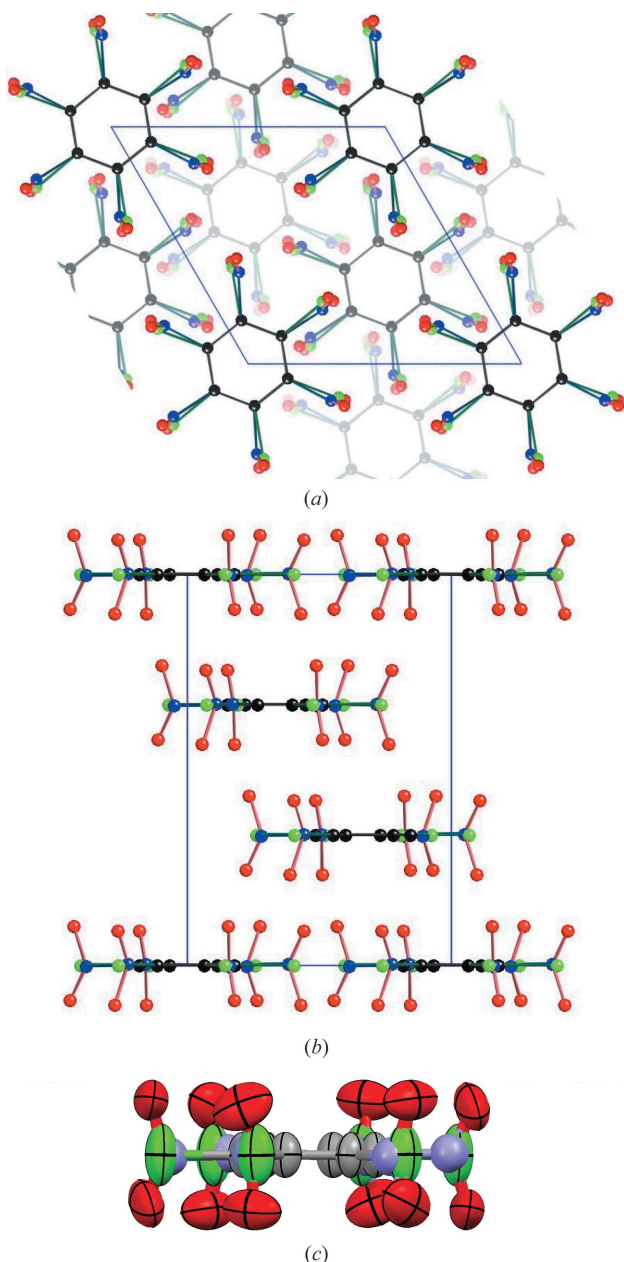**Table 1**
Cell data for pentachloronitrobenzene, $C_6Cl_5NO_2$ (PCNB), derived from X-ray diffraction at 298 K.

Space group	Z	a (Å)	b (Å)	c (Å)	γ (°)
$R\bar{3}$	3	8.773 (1)	8.773 (1)	11.258 (2)	120

PCNB is one of a series of chloronitrobenzene derivatives that are currently being studied because their disordered nature and propensity to undergo phase transitions are

Figure 1
The average structure of PCNB. Each of the six substituent sites in every molecule contains $\frac{1}{6}$ NO$_2$ and $\frac{5}{6}$ Cl. (*a*) View down [001]; (*b*) view down [100]; (*c*) drawing of the molecule showing atomic displacement ellipsoids at the 50% probability level, as derived from the X-ray diffraction structure determination at 298 K.

thought to be responsible for their anomalous dielectric properties (Hall & Horsfall, 1973). Disorder often strongly affects the electronic environment in such materials and it is considered that this may be fundamental to physical properties such as, for example, second harmonic generation (Cole *et al.*, 2000). Our goal is to quantify the disorder and short-range order as fully as possible with a view to being able to control or harness such disorder and aid the design of new functional molecular materials.

Although many pentachlorobenzene derivatives have been found to exhibit disorder at room temperature (Hall & Horsfall, 1973; Tanaka *et al.*, 1974; Khotsyanova *et al.*, 1969; Sakurai, 1962), this disorder is often difficult to characterize fully using conventional crystallography since this only gives information on the *average* structure of the material. The overlapping electron density that results from the averaging in a disordered material can lead to uncertainties both with the assignment of accurate atomic positional parameters and with the determination of occupancy factors. In a recent paper we have reported conventional crystallographic studies of PCNB as a function of temperature using both X-ray and neutron diffraction (Cole *et al.*, 2007). These studies have revealed that each molecular site in PCNB contains the molecule in one of six different orientations, each with equal probability of occurrence, giving the molecular site full sixfold symmetry on average. Moreover the variable-temperature studies indicated that the disorder does not change substantially from room temperature down to 5 K with the possible exception of a reduction in the degree of libration of the nitro group. Fig. 1 shows drawings of the average structure. Cell data are given in Table 1 for reference.

Note in Fig. 1(*c*) how the atomic displacement parameters derived from the average structure determination show unusual elongation of the C and Cl atoms normal to the molecular plane. This may be an indication of the molecular displacements and tilts from this plane that are described later.

Potential energy calculations have been used to model the disorder in PCNB using rigid-body atom-pair interaction potentials. The potential energy profile was found to have six equal minima suggesting sixfold rotation of the molecules (Gavezzotti & Simonetta, 1975). Dielectric permittivity measurements suggested that the disorder becomes rigid at 200 K (Kolodziej *et al.*, 1999), and a glass transition which is dependent on the rate of cooling has been observed at approximately 190 K (Shahin & Murthy, 2003; Correria *et al.*, 2002).
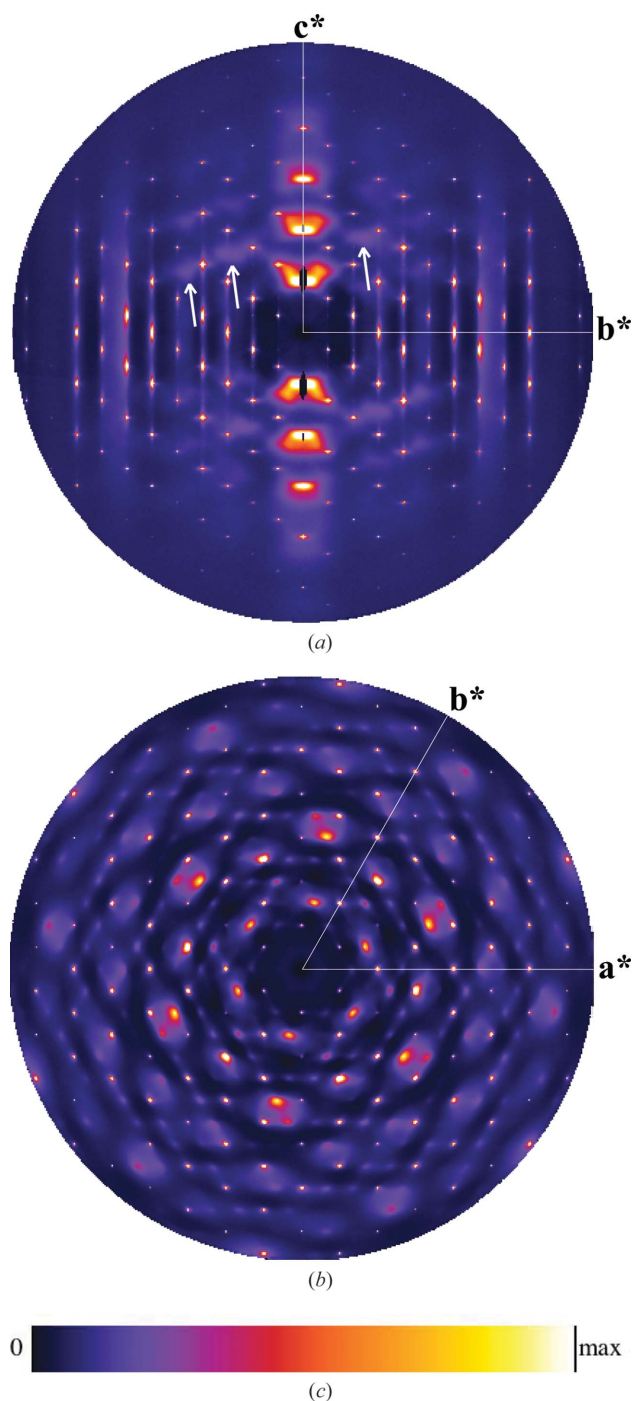
2. Diffuse scattering data

Diffuse scattering data have been recorded using both X-ray and neutron sources. The most detailed images have been recorded using X-rays where the much greater flux available and low beam divergence allowed much better quality (high-resolution, low-noise) patterns to be recorded. However recording neutron diffuse scattering was also attempted as PCNB has the most unusual property for an organic compound that it contains no hydrogen. This is a most desir-

able property for neutron scattering since the presence of hydrogen produces a very high incoherent signal which may far exceed the diffuse elastic scattering. Another advantage of using neutrons is that it allows contrast between different elements markedly different from that available in X-ray experiments and it was considered that a comparative study could aid in the analysis of the PCNB disorder. These measurements were carried out using the time-of-flight


(a)

(b)

(c)

Figure 2
Observed X-ray diffuse scattering data, recorded on beamline 1-ID-C at the Advanced Photon Source (APS). (a) 0kl section; (b) hk0 section.

neutron Laue diffractometer SXD at the ISIS Spallation Neutron Source, Rutherford Appleton Laboratory, Oxon, UK (Keen *et al.*, 2006). Exploratory neutron diffraction measurements have also been undertaken using D10 at the Institut Laue–Langevin, Grenoble, France (Cole *et al.*, 2007). Preliminary X-ray experiments were carried out on Station 9.8 at the Synchrotron Radiation Source, Daresbury, UK. These were carried out at three different temperatures: 100, 180 and 293 K. These initial measurements confirmed the presence of strong, structured diffuse scattering in the title material (Thomas, 2007) and set the framework for the subsequent experiments described below. In addition, the consistent appearance of the diffuse scattering in the multiple-temperature measurements from Station 9.8 indicated the source of this scattering to be static molecular disorder rather than dynamic effects.

Subsequently, a complete three-dimensional set of diffuse scattering data of better quality (high-resolution, low-noise) was obtained using the high-energy beamline 1-ID-C at the Advanced Photon Source (APS) using a similar procedure to that described in earlier papers (Welberry *et al.*, 2005; Goossens *et al.*, 2005). Data were collected in the form of 508 individual 2 s exposures on a Mar 345 image-plate detector using small ($0.36°$) oscillations, a wavelength of $\lambda = 0.30996$ Å and a sample-to-detector distance of 292.36 mm. This gave data out to a maximum $\sin \theta/\lambda$ of 0.85 Å^{-1}. Data from individual frames were combined using the median intensity within each frame as a scale and a background (due to air scattering) was subtracted. Finally, two-dimensional plane sections of data normal to particular crystal directions were extracted from the three-dimensional data using the program *EXCAVATE* (Estermann & Steurer, 1998). These data confirmed the general appearance of the diffuse features observed in the preliminary Station 9.8 and SXD measurements, but put these on a more quantitative basis, appropriate for quantitative modelling. Fig. 2 shows the data for the 0kl and hk0 sections. These two sections show strong and highly structured diffuse scattering and were chosen for use in the analysis reported here.

The most striking feature of the 0kl data is the column of very strong and asymmetric diffuse blobs that occur near the Bragg hkl positions $0\,0\,3$, $0\,0\,6$, $0\,0\,9$ and $0\,0\,12$. The blob around $0\,0\,3$ is particularly striking in that it has the appearance of a *butterfly* with distinct wings. A second set of much weaker peaks (some of which are indicated with arrows in Fig. 2a) are clearly visible and these are not associated with Bragg peaks. A third set of distinctive features consists of the narrow diffuse bands of scattering that run vertically along columns of Bragg peaks (*i.e.* lines of constant k). These are most noticeable for k = 3, 4, 6, 7 and 9. Finally, a small additional feature may be seen on close scrutiny; at some Bragg positions, the aforementioned diffuse bands are crossed by small horizontal streaks protruding from the Bragg positions. The most striking feature of the hk0 data is the hexagonal pattern of broad diffuse peaks. This pattern is oriented at $\sim 8.5°$ to the vertical and is clearly related to the Fourier transform of the basic molecular shape. Within each of these broad peaks, however,

it is seen that the scattering bunches up into much sharper diffuse peaks that are centred around Bragg positions. These smaller peaks are fairly isotropic, although there is some tendency for them to be more elongated along directions normal to the radial vector from the origin than along it.

3. Monte Carlo model

Our methods for analysing diffuse scattering from disordered crystals are now well established (Welberry, 2004). The methods, which are widely applicable to a diverse range of materials, use Monte Carlo (MC) simulation of a model crystal to try to reproduce observed scattering patterns. A model crystal is built using harmonic springs to mimic intermolecular interactions and torsional springs to mimic intramolecular forces. In addition, occupational variables can be used to model distributions of different atomic or molecular species or their basic orientations. The parameters that describe a given model may include the spring constants themselves, the spring lengths, constants describing the interaction between neighbouring occupancy variables and size-effect variables which enable the lengths of springs to be coupled to the occupancy of the species they link, so producing the possibility of local relaxation.

MC simulation is first carried out using a starting set of model parameter values and then diffraction patterns are computed corresponding to the observed sections of data.

(a)

(b)
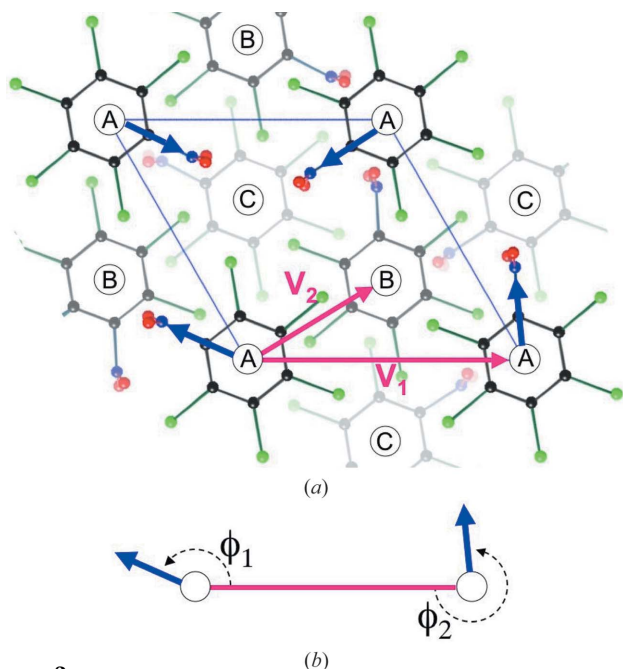
Figure 3
The disordered structure of PCNB showing the three different molecular layers A, B and C, which are stacked in an ABCABC···c.c.p.-type sequence. (a) A small region of structure with each molecular site randomly occupied by one of six different possible molecular orientations. The orientation of a given molecule is defined by a vector (shown in blue) directed from the molecular centre towards the NO_2 group. (b) The two angles, ϕ_1 and ϕ_2, which define the mutual orientation of neighbouring pairs of molecules, are defined.

After comparison with the observed data the parameters are adjusted and a new simulation is carried out. This process is then continued iteratively until a satisfactory match between observed and calculated patterns is obtained. The advantage of the method is that it can be applied generally to all systems regardless of their complexity or the size of the atomic displacements that might be present. The only limitation is the extent to which the MC energy can be made to realistically represent the real system energy. At one extreme, a very simplified model may be useful to demonstrate particular qualitative effects (Welberry, 2001), while at the other a quantitative and very detailed description of a disordered structure can be obtained (Welberry et al., 2001).

In the present study modelling of the disorder in PCNB was carried out in two stages:

(i) ordering of the basic molecular orientations on the sites of the *average* lattice and

(ii) subsequent relaxation of the molecular positions and orientations to alleviate any stresses caused by local misfit of the molecules.

The model was based on the molecular conformation and crystal lattice positions of the average structure determined at room temperature.

3.1. Occupancy ordering

Fig. 3(a) shows a drawing of a representative portion of the disordered structure viewed down c. Three different superposed layers of molecules (labelled A, B and C) are shown with different levels of shading. Each molecular site contains one of the six different basic molecular orientations. For the top-most layer, corresponding to molecules residing on the cell corners, the orientation is indicated by the blue arrows which point from the centre of the molecule towards the NO_2 group. Also indicated in this figure are the two different types of near-neighbour intermolecular vectors, $\mathbf{V}_1$ and $\mathbf{V}_2$. $\mathbf{V}_1$ is between two molecules within one molecular plane and $\mathbf{V}_2$ is between molecules in neighbouring molecular planes.

In order to induce short-range ordering of the molecular orientations, we use a MC energy of the form

$$E_{occ} = \sum_{\text{all vectors, } \mathbf{V}_1} \Psi_{i,j} + \sum_{\text{all vectors, } \mathbf{V}_2} \Omega_{i,j}. \qquad (1)$$

Here, $\Psi_{i,j}$ and $\Omega_{i,j}$, respectively, are interactions that depend on the mutual orientations of the two molecules i and j that are linked by the vector $\mathbf{V}_1$ or $\mathbf{V}_2$, respectively. Fig. 3(b) shows how the mutual orientation can be defined in terms of the two angles ϕ_1 and ϕ_2 that define the angle that is made by the blue vector and the interaction vector ($\mathbf{V}_1$ in this case). Since molecules i and j can each take any one of six different orientations, there are 36 different combinations of ϕ_1 and ϕ_2, and hence 36 possible values for $\Psi_{i,j}$ and $\Omega_{i,j}$. These different possibilities for the cases of $\mathbf{V}_1$ and $\mathbf{V}_2$ vectors are given in Tables 2 and 3, respectively.

However, since it is only the mutual orientation that matters, the values of $\Psi_{i,j}$ and $\Omega_{i,j}$ form symmetric matrices such that $\Psi_{i,j} = \Psi_{j,i}$ and $\Omega_{i,j} = \Omega_{j,i}$, and hence there are in

Table 2
Values of the angles, ϕ_1 and ϕ_2 (°), defining the different possible interactions, $\Psi_{i,j}$, along nearest-neighbour in-plane vectors of type $\mathbf{V}_1$.

	$j = 1$	$j = 2$	$j = 3$	$j = 4$	$j = 5$	$j = 6$
$i = 1$	40, 40	40, 100	40, 160	40, 220	40, 280	40, 340
$i = 2$	100, 40	100, 100	100, 160	100, 220	100, 280	100, 340
$i = 3$	160, 40	160, 100	160, 160	160, 220	160, 280	160, 340
$i = 4$	220, 40	220, 100	220, 160	220, 220	220, 280	220, 340
$i = 5$	280, 40	280, 100	280, 160	280, 220	280, 280	280, 340
$i = 6$	340, 40	340, 100	340, 160	340, 220	340, 280	340, 340

Table 3
Values of the angles, ϕ_1 and ϕ_2 (°), defining the different possible interactions, $\Omega_{i,j}$, along nearest-neighbour between-plane vectors of type $\mathbf{V}_2$.

	$j = 1$	$j = 2$	$j = 3$	$j = 4$	$j = 5$	$j = 6$
$i = 1$	10, 10	10, 70	10, 130	70, 190	10, 250	10, 310
$i = 2$	70, 10	70, 70	70, 130	70, 190	70, 250	70, 310
$i = 3$	130, 10	130, 70	130, 130	130, 190	130, 250	130, 310
$i = 4$	190, 10	190, 70	190, 130	190, 190	190, 250	190, 310
$i = 5$	250, 10	250, 70	250, 130	250, 190	250, 250	250, 310
$i = 6$	310, 10	310, 70	310, 130	310, 190	310, 250	310, 310

Table 4
Z-matrix representation of the molecule used in the analysis.

Atom, i	Symbol	j	$d_{i,j}$	k	$\rho_{i,j,k}$	l	$\zeta_{i,j,k,l}$
1	C1	–	–	–	–	–	–
2	C2	1	1.38	–	–	–	–
3	Cl2	2	1.72	1	119.2	–	–
4	C3	2	1.38	3	120.7	1	179.6
5	Cl3	4	1.72	2	119.2	3	0.4
6	C4	4	1.38	5	120.7	2	−179.6
7	Cl4	6	1.72	4	119.2	5	−0.4
8	C5	6	1.38	7	120.7	4	179.6
9	Cl5	8	1.72	6	119.2	7	0.4
10	C6	8	1.38	9	120.7	6	−179.6
11	Cl6	10	1.72	8	119.2	1	179.6
12	N1	1	1.55	10	126.0	2	178.9
13	O2	12	1.23	1	106.2	10	80.0
14	O1	12	1.07	13	135.6	1	162.5

each only 21 independent interactions. Even so, a parameter space comprising these 42 different possible interaction variables presents a formidable challenge when a solution which reproduces the observations is sought.

3.2. Size-effect relaxation

The second stage of the MC simulation is to allow size-effect relaxation of the distribution of molecules resulting from the ordering of occupancies described above. Our aim here is to mimic the real intermolecular interactions with a (relatively) small set of interatomic contact vectors that is sufficient to define both the separation and mutual orientation of neighbouring molecules.

First we describe the positions of all the atoms of a given molecule using a z-matrix description of the molecular geometry. This method, commonly used for example in *ab initio* molecular-orbital calculations (see *e.g.* Hehre *et al.*,

1986), allows the geometry of the molecule to be specified in terms of bond lengths, bond angles and dihedral angles. The z matrix used in the present study is given in Table 4. At the outset of the study it was intended that the molecule was to be treated as a rigid body, but with the possibility that the NO_2 group was able to rotate. This possibility could be achieved simply by allowing the torsional angle, defining the angle made by the plane of the NO_2 group with that of the benzene ring, to be a variable. For the present preliminary study, however, this possibility was not invoked and the whole molecule was treated as strictly rigid. The position of the molecule in the model crystal was defined using three centre-of-mass coordinates (x, y, z) and a quaternion (q_1, q_2, q_3, q_4) defining its orientation.

Intermolecular interactions were mimicked by interatomic interactions acting only between the Cl and N atoms of neighbouring molecules. Only five basic types of such contacts were used and these are shown in Fig. 4. Contacts P and Q are between nearest-neighbour in-plane molecules while R, S and T are between nearest-neighbour molecules in adjacent planes. Table 5 gives details of the interatomic (NN, NCl, ClN or ClCl) contact distances, l_i^{ab}, obtained using the coordinates from the *average* (Bragg) structure determination, for each of these five types of contact.

In order to allow for atomic displacements in the MC simulation, including those due to thermal motion and size-effect relaxation, we use an energy, E_{disp}, comprised of a set of harmonic (Hooke's law) springs

$$E_{disp} = \sum_{i=1}^{5} \sum_{\text{types ab}} k_i (d - d_i^{ab})^2. \quad (2)$$

Here d is the instantaneous length of a particular interatomic vector. k_i are spring force constants with unique values for each of the five different types of contact, i. Similarly, d_i^{ab} are equilibrium spring lengths which depend not only on the type of contact, i, but also on the particular pair of atoms, ab, that take part in the contact, *i.e.* ab may be NN, NCl, ClN or ClCl. These values of the spring lengths are defined relative to the vector distances, l_i^{ab}, in the average structure (see Table 5) and are formulated in terms of parameters which describe the local perturbations due to the size effect

$$d_i^{ab} = l_i^{ab}(1 + \epsilon_i^{ab}). \quad (3)$$

Here ϵ_i^{ab} are size-effect parameters which may take different values for ab = NN, NCl, ClN or ClCl and for each different contact i. If p_i^{NN}, p_i^{NCl} *etc.* are the proportions of the different types of interatomic vector that comprise a particular intermolecular contact then, in order for the average interatomic distances to be maintained, it is necessary that

$$p_i^{NN}\epsilon_i^{NN} + p_i^{NCl}\epsilon_i^{NCl} + p_i^{ClN}\epsilon_i^{ClN} + p_i^{ClCl}\epsilon_i^{ClCl} = 0. \quad (4)$$

Although this is the only condition that it is necessary to impose on the size-effect parameters in the present work we have also imposed the further two conditions

$$\epsilon_i^{NCl} = \epsilon_i^{ClN} \quad \text{and} \quad \epsilon_i^{NN} = 2 \times \epsilon_i^{NCl}. \quad (5)$$

Table 5
The five basic types of intermolecular vector and the different interatomic distances, l_i^{ab}.

These values for l_i^{ab} (Å) were obtained from the coordinates of the *average* structure (see Fig. 3).

Vector	N···N	N···Cl	Cl···N	Cl···Cl
P	3.759	3.544	3.782	3.577
Q	4.193	3.937	3.937	3.680
R	3.817	3.919	3.919	4.035
S	4.315	4.232	4.278	4.203
T	4.385	4.234	4.435	4.277

The first of these two conditions is a statement that the length of the contact is the sum of the size of the two contributing species and is not dependent on the order in which they occur. The second condition is simply a reflection of the fact that if the size of the NO_2 group is bigger than Cl then a Cl···N contact will be lengthened relative to a Cl···Cl contact by this difference and if both Cls are replaced by NO_2, then the contact distance will be increased by twice as much. With the three conditions given by (4) and (5), this leaves just a single size-effect parameter, ϵ_i^{NN} say, for each of the five types of contact.

As an example, consider a random distribution in which each site of a pair of neighbouring molecular sites contains a molecule in one of six different orientations quite indepen-

(a)

(b)
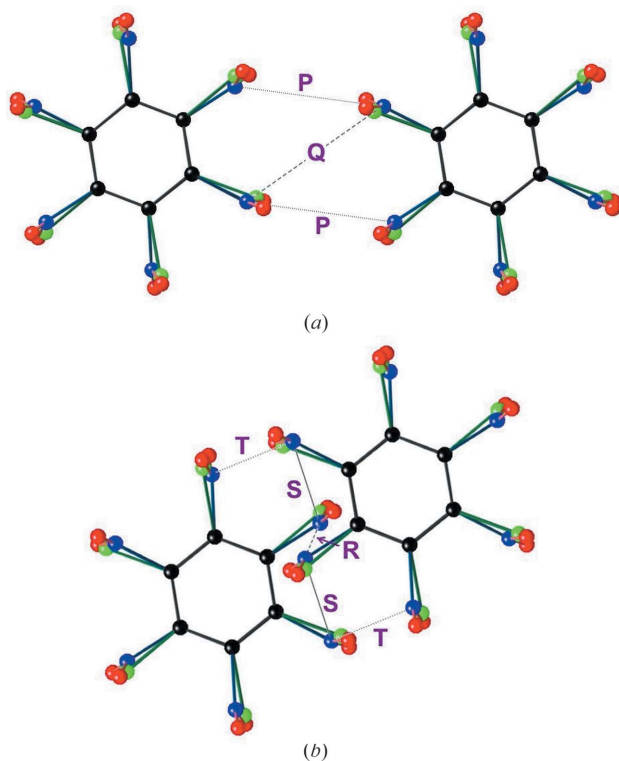
Figure 4
The five different intermolecular interaction vectors used in the MC simulation: (*a*) within the molecular planes; (*b*) between neighbouring molecular planes. See Table 5.

dently. The probabilities of a given intermolecular vector comprising NN, NCl, ClN or ClCl contacts are then

$$p_i^{NN} = \frac{1}{36}; \qquad p_i^{NCl} = p_i^{ClN} = \frac{5}{36}; \qquad p_i^{ClCl} = \frac{25}{36}. \quad (6)$$

Hence (4) becomes

$$\epsilon_i^{NN} + 5\epsilon_i^{NCl} + 5\epsilon_i^{ClN} + 25\epsilon_i^{ClCl} = 0 \quad (7)$$

and substituting from (5)

$$\epsilon_i^{NN} + 5\epsilon_i^{NN} = -25\epsilon_i^{ClCl}, \quad (8)$$

whence

$$\epsilon_i^{ClCl} = -\frac{6}{25}\epsilon_i^{NN} \quad \text{and} \quad \epsilon_i^{ClN} = \frac{1}{2}\epsilon_i^{NN}. \quad (9)$$

For the present study, therefore, five independent spring constants, k_i, together with a single size-effect parameter, ϵ_i, associated with each were the only parameters used in the analysis.

3.3. MC simulation

MC simulations were carried out in two distinct stages, as detailed in the previous subsections. In all cases the simulation model comprised a three-dimensional crystal with molecules specified by indices i, j, k to identify the unit cell and a fourth index, L, to identify the molecular site within the cell. For preliminary studies, particularly in exploring the occupational parameter space, only small crystals were used with maximum values of i, j, k of only 12 or 16, but for later parts of the study, where high-quality calculated diffraction patterns were required, this was increased to 48. In these final simulations, the crystal therefore comprised $48 \times 48 \times 48 \times 3 = 331\,776$ molecules.

The normal MC algorithm (Metropolis *et al.*, 1953) was used as follows. A site in the crystal was chosen at random and the set of eight variables defining the conformation (1 torsion angle), orientation (4 quaternion variables) and centre of mass (x_c, y_c, z_c) of the molecule, was subjected to a small random increment. The contribution to the energy of all terms that are dependent on the altered variables was computed before and after the change was made. The energy difference, $\Delta E = E_{new} - E_{old}$, was used to decide whether the new configuration should be kept, or the system returned to the original configuration. A pseudo-random number, η, chosen uniformly in the range [0, 1], was compared with the transition probability, $P = \exp(-\Delta E/kT)$, where T is the temperature and k Boltzmann's constant. If $\eta < P$ the new configuration was accepted, while if $\eta > P$ it was rejected and the system returned to the original state. A MC cycle is defined as that number of such individual steps needed to visit each site once on average. In the present work we assumed $kT = 1$ throughout and consequently the force constants determined were relative to this energy scale. For the preliminary occupancy ordering simulations, a relatively small number of MC cycles were used simply to establish different ordering patterns, but for the second-stage MC simulations, using (2),

1000 cycles were used in order to allow the system to closely approach equilibrium.

To calculate the diffraction pattern from the output of the MC runs, we used the program *DIFFUSE* (Butler & Welberry, 1992). This algorithm obtains the diffraction pattern by taking the average of a large number of diffraction patterns calculated from small regions (or 'lots'), picked at random, from the simulated real-space array. This has the effect of removing the high-frequency noise, which necessarily occurs if a single calculation from the whole simulated array is performed. It is only necessary that the 'lot size' is large enough to include all significant non-zero correlations. For the patterns shown later a 'lot size' of $12 \times 12 \times 12$ was used and the patterns were averaged over 400 such 'lots'. Since, at this level of compu-

tation, each part of the model crystal is sampled more than twice on average, these calculations represent something close to the best that can be obtained from the chosen simulation crystal size of $48 \times 48 \times 48$ unit cells; any further improvement would require a larger crystal size.

4. Results and discussion

4.1. Occupancy ordering

As was described in §3.1, complete exploration of the parameter space detailed in Tables 2 and 3 is a virtually impossible task. A considerable amount of time and effort was expended trying to find values for particular interactions $\Psi_{i,j}$ and $\Omega_{i,j}$ that would produce distributions of molecular orientations with calculated diffraction patterns showing some similarity to the observed patterns. While it was supposed, from the outset, that the strong diffuse peaks around the 0 0 3, 0 0 6 and 0 0 9 Bragg positions were of a displacement origin, it seemed likely that the broader features of the patterns indicated by the arrows in Fig. 2 were due to the occupancy disorder. A number of different strategies were adopted.

Firstly, a relatively small number of patterns were computed on the supposition that some particular nearest-neighbour pairs of molecules would be energetically strongly favoured (or disfavoured), *e.g.* ones where two NO_2 groups were in close proximity. Next, a more systematic approach was adopted where simulations were carried out in which each of the 42 possible interactions was given, in turn, a positive or negative value while all others were zero. Then some combinations of interactions were chosen by inspection in order to try to induce a tendency for the formation of particular types of superlattice ordering, hence allowing for some kind of a micro-twinning solution. Finally, a simple genetic algorithm was set up to search the 42 parameter space in order to try to find solutions that would produce diffuse intensity in particular regions of the diffraction pattern corresponding to the observations. All of these strategies failed to produce any diffraction patterns that convincingly reproduced the observed features indicated by the arrows in Fig. 2(*a*), although a small number did appear to show some promise.

In Fig. 5 we show a selection of different diffraction patterns that have been chosen to indicate the diversity that is possible, including some particular ones that showed initial promise. The calculated patterns were obtained using small crystal sizes and inexpensive *DIFFUSE* calculations, but nevertheless they clearly show the important features.

The diffraction pattern of Fig. 5(*d*) was considered most promising as the horizontally elongated diffuse blobs that occur in rows sloping from the top-right to the bottom-left of the figure had something of the character of the diffuse regions indicated by the arrows in Fig. 2(*a*). However, the rather sharp diffuse peaks that occur near the centre of the pattern do not have any counterpart in the observed pattern. They are positioned either side of where the large diffuse peaks associated with the 0 0 3 and 0 0 6 Bragg positions occur in the observed patterns, and it seemed not inconceivable that
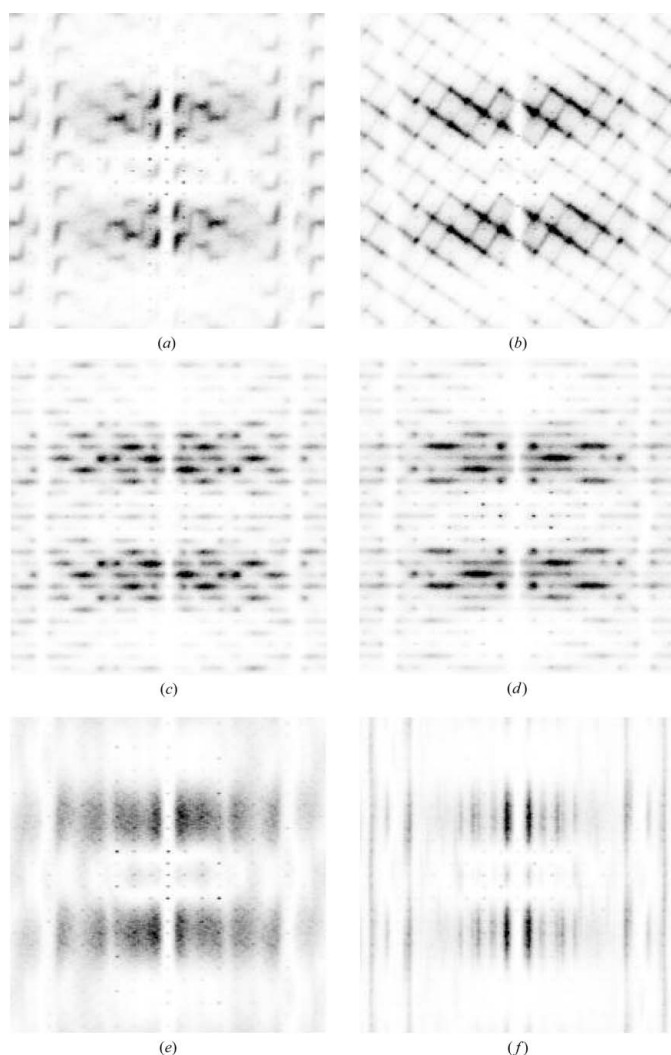
Figure 5
Example diffraction patterns (0*kl* section) corresponding to different examples of occupancy order. For these patterns there was no displacement disorder. (*a*)–(*d*) Examples where $\Omega_{i,j}$ for a single type of molecular pair was given a negative value, while all other interactions were zero. (*e*) and (*f*) Examples where only one or more $\Psi_{i,j}$ interaction was given negative energies. (*e*) A single type of pair, whereas (*f*) corresponds to three different types in combination. The patterns were: (*a*) $\Omega_{2,6} = -1.0$; (*b*) $\Omega_{2,5} = -1.0$; (*c*) $\Omega_{1,2} = -1.0$; (*d*) $\Omega_{1,6} = -1.0$; (*e*) $\Psi_{1,1} = -1.0$; (*f*) $\Psi_{1,2} = \Psi_{3,5} = \Psi_{4,6} = -1.0$.

they could have been subsumed by these peaks once displacement effects were introduced. On further investigation, however, it was found that the exact positions of the rows of blobs in the MC simulation were incorrect. Moreover, the pairs of sharper peaks persisted even when displacement disorder was present.

4.2. Size-effect relaxation and displacement disorder

Since no satisfactory solution involving occupancy short-range order (SRO) could be found, attention was turned to the possibility that the observed diffraction features were being produced entirely from displacements induced by size effects caused by the large differences between the NO_2 and Cl groups. These size effects are a consequence of the formation of close intermolecular contacts (less than the sum of the van der Waal's radii) between NO_2 groups on neighbouring molecules and NO_2 and Cl close contacts. The inclusion of such effects can be justified from the average structure in the form of the elongated thermal motion affecting the backbone of the molecule (cf. Fig. 1). Consequently, for this part of the study it was assumed that there were no occupancy correlations and simulations were carried out using the MC energy of the form given in (2) with a random distribution of occupancies.

The five spring constants, k_i, were initially made to be all equal. It was further assumed that size-effect distortions would be most pronounced along vector types **R** and **S** in Fig. 4, where NO_2 groups on neighbouring molecules might most closely come into contact. Size-effect parameters, ϵ_i, were only given non-zero values along these two types of vector. As the MC simulation progressed, various lattice averages were computed in order to assess convergence to an equilibrium state. Among these was a measure of the mean-squared amplitude of atomic displacements, $B_{iso} = 8\pi^2 \overline{u^2}$, where u are atomic displacements away from their average positions. This measure of B_{iso} was used to provide a feedback mechanism to allow the magnitudes of the spring constants to be all rescaled during iteration so that the final value of B_{iso} achieved in the simulation could be directed towards some predetermined value. With this mechanism in place, the effect of adjusting the relative magnitudes of different spring constants and of adjusting the two size-effect parameters was explored.

Fig. 6 shows computed diffraction patterns for the $0kl$ and $hk0$ sections of the final model arrived at as a result of this exploration. For each section the upper semi-circle shows the calculated pattern, while the lower semi-circle is of the corresponding observed data for comparison. Table 6 lists the values for the spring constants and size-effect parameters used for this simulation. Comparison of the calculated patterns with the observed data shows that the model gives excellent agreement and reproduces all of the different features identified in §2, even the small horizontal streaks emanating from some Bragg peaks (indicated by the arrows in Fig. 6a). The exploration of the parameter space revealed several key factors, which determine the details of the pattern.

Firstly, the size-effect parameters ϵ_R^{NN} and ϵ_S^{NN} are responsible for the strong asymmetry of the strong diffuse peaks around 003, 006 etc. and must be both large and positive, indicating that the NO_2 groups take up much more space than is available in the average structure. The actual magnitudes for these size-effect parameters also govern the way that the series of peaks 003, 006, 009 and 0012 progressively

(a)

(b)

(c)
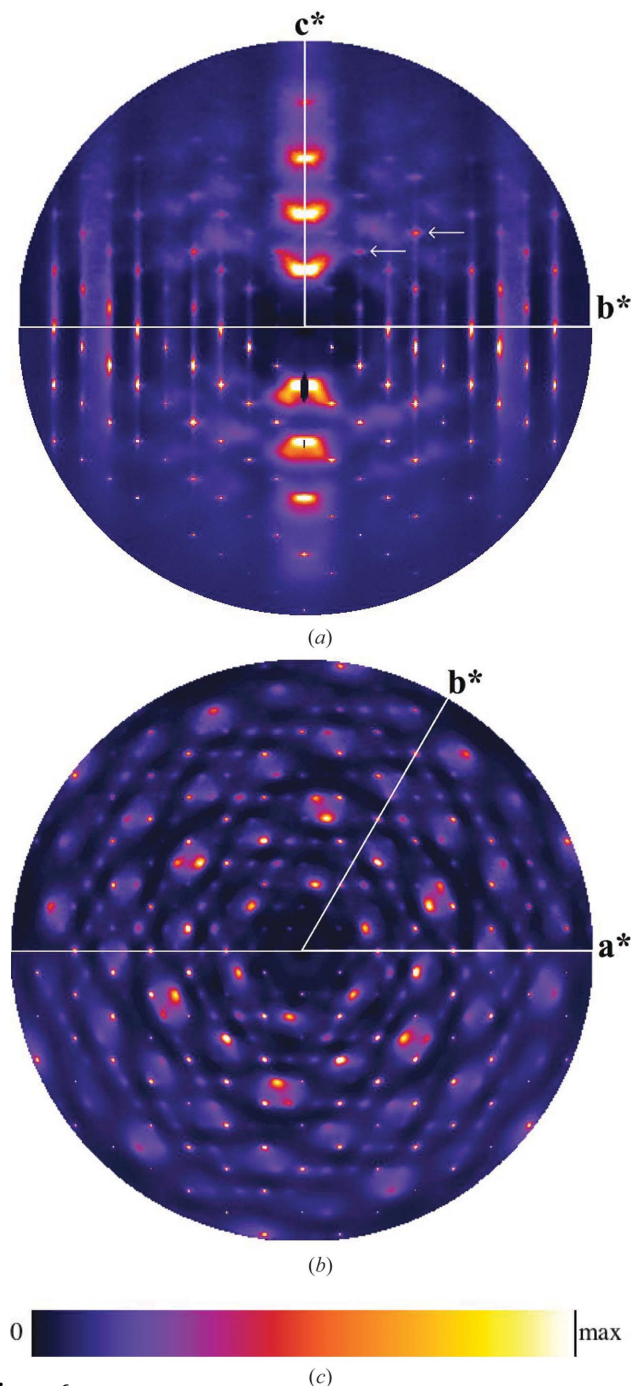
Figure 6
Calculated diffuse scattering patterns (upper semi-circles) compared with the corresponding observed X-ray data (lower semi-circles). (a) $0kl$ section; (b) $hk0$ section. [Note the upper and lower halves are not related by m symmetry. $0kl$ has twofold symmetry; $hk0$ has sixfold symmetry. It should also be noted that the calculated patterns contain no actual Bragg peaks since the average structure is subtracted during the calculation].

Table 6
The force constants, k_i, and size-effect parameters, ϵ_i, used for the simulation whose diffraction patterns are shown in Fig. 6.

The k_i are in units of kT and the ϵ_i are in Å. Note that for each vector the four values of ϵ_i satisfy equation (9).

Vector type	k_i	ϵ^{NN}	ϵ^{NCl}	ϵ^{ClN}	ϵ^{ClCl}
P	3.94	0.0	0.0	0.0	0.0
Q	3.94	0.0	0.0	0.0	0.0
R	2.62	+1.5	+0.75	+0.75	−0.36
S	2.62	+2.0	+1.0	+1.0	−0.48
T	1.31	0.0	0.0	0.0	0.0

Table 7
The effect of size on atom–atom vectors comprising the intermolecular vector **R** (see Fig. 4; distances given in Å).

Vector type	Average structure	Mean	σ	Δd	% change
N$\cdots$N	3.817	4.404	0.27	0.587	+15
N$\cdots$Cl	3.919	4.201	0.27	0.282	+7
Cl$\cdots$N	3.919	4.201	0.27	0.282	+7
Cl$\cdots$Cl	4.035	3.951	0.27	−0.084	−2

diminish in intensity. For smaller values of the parameters, the asymmetry is still pronounced but the 0 0 9 and 0 0 12 peaks are much stronger.

The narrow diffuse bands of scattering that run vertically along columns of Bragg peaks in Fig. 6(a) (i.e. lines of constant k, particularly for k = 3, 4, 6, 7 and 9), are influenced by the magnitude of the in-plane force constants, k_P and k_Q. If these force constants are reduced in magnitude, the vertical streaking becomes less pronounced and the thermal diffuse scattering (TDS) very close to the Bragg peaks becomes less elongated along the c^* direction.

The broad diffuse peaks indicated by the arrows in Fig. 2(a) are also well reproduced in the calculated patterns, both in position and their relative magnitude to the strong asymmetric peaks. These peaks have arisen quite naturally out of the molecular displacements that have occurred. There is some suggestion that their shape is not quite right and it is possible that this could be influenced by the presence of some small degree of occupancy SRO. However, the overall agreement of the current model, which has random occupancies, is so good and the number of different possible ways in which a small amount of SRO could occur is so large that it seems very unlikely that a better model could easily be found.

4.3. Atomic distributions

It is informative to look at the distribution of atomic positions resulting from the MC simulation. In Table 7, we give average contact distances for the different types of atom pairs for the intermolecular vector R. The first column in the table gives the distance calculated from the average sites determined in the Bragg structure refinement, while the second column gives the value in the MC simulated crystal. This clearly shows how the average N$\cdots$N distance has increased relative to the average structure value by $\sim$ 0.6 Å, the average

N$\cdots$Cl distance has increased by $\sim$ 0.3 Å, while the average Cl$\cdots$Cl distance has decreased by $\sim$ 0.08 Å. This is consistent with the displacements represented by the atomic displacement parameters arising from the average structure determination. In fact, the distribution of atomic position plots exhibit a similar form to the observed thermal ellipsoids. It should be noted that these figures are substantially less than the actual size-effect parameters, ϵ_i, that were used to induce the effects. This is consistent with our findings in numerous previous studies involving size effect.

The same effect is shown graphically in Fig. 7. Fig. 7(a) shows superposed the atom positions in all unit cells in which the R intermolecular contact between molecules in the layers at $\frac{1}{3}c$ and $\frac{2}{3}c$ comprises an N$\cdots$N interatomic contact. In contrast, Fig. 7(b) shows superposed the atom positions in all unit cells in which the R intermolecular contact comprises a Cl$\cdots$Cl interatomic contact. In fact, this plot is of only those molecules where these Cl groups are para- to the NO$_2$ group. The scatter plot of Fig. 7(a) clearly shows how two NO$_2$ groups have tilted away from each other. The plot of Fig. 7(b), on the other hand, shows a slight tilting of the Cl groups toward each other. Finally, Fig. 7(c) shows the distribution of interatomic contact distances that comprise the R intermolecular contact, again graphically reflecting the same information given in Table 7. Note how, because there are many more Cl$\cdots$Cl contacts in the whole crystal than there are other types, the average for Cl$\cdots$Cl is only slightly less than the overall average.

5. Conclusions

In this paper we have described a simple MC model that reproduces in detail the diffraction patterns that have been observed for PCNB. After an extensive search of the parameter space that is required to specify SRO of the six different basic molecular orientations, it has been concluded that virtually no such occupancy correlations are present. The strong, detailed and very distinctive diffraction patterns can be accounted for almost entirely on the assumption of the random occupancy of each molecular site, but with very large local relaxation displacements that tend to increase the neighbouring distances for contacts involving NO$_2\cdots$NO$_2$ and NO$_2\cdots$Cl with a corresponding reduction for those involving Cl$\cdots$Cl.

This result is rather surprising. The magnitude of the size-effect displacements that are present are very large. An increase in the NO$_2\cdots$NO$_2$ distance of $\sim$ 0.6 Å corresponds to a local distortion of $\sim$ 16% when compared with the basic spacing of the intermolecular layers (3.75 Å). Although NO$_2\cdots$NO$_2$ contacts occur relatively rarely, even the much more frequently occurring NO$_2\cdots$Cl contacts are increased by $\sim$ 8% of the layer spacing. To achieve these magnitudes of distortion the molecules must be very uncomfortable in the average structure geometry. It is therefore surprising that the system chooses to pack this way rather than find an energy minimum defining a different crystal structure which will accommodate the differently sized substituents in a more
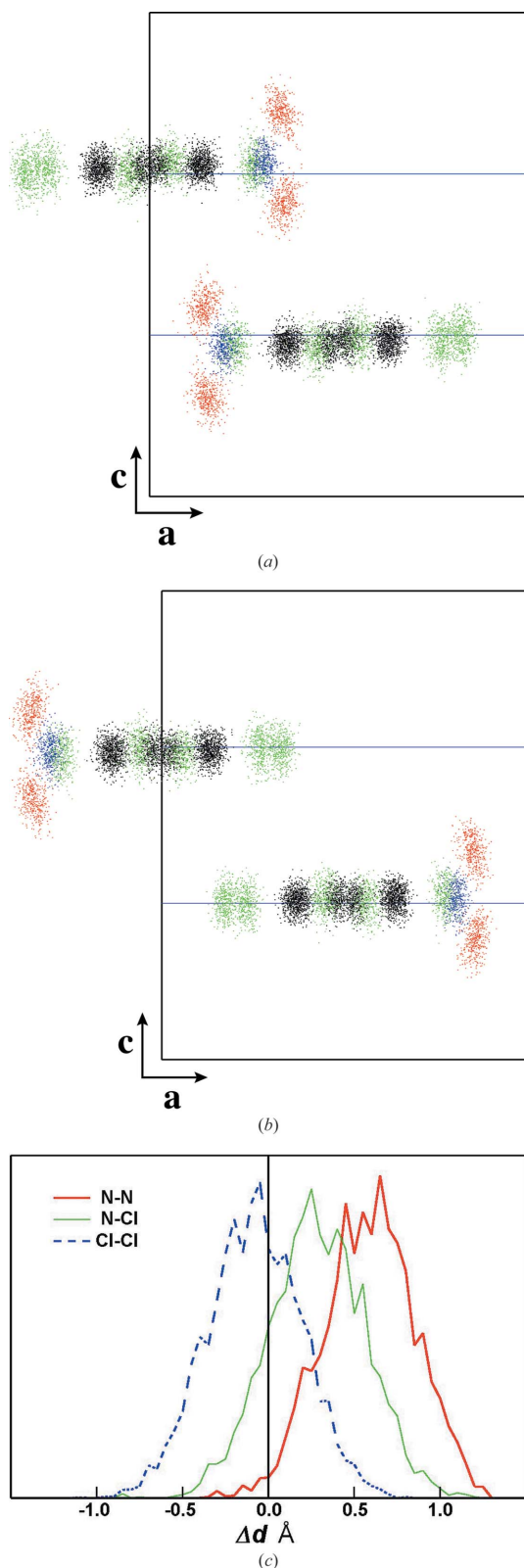
Figure 7
Scatter plots viewed down **b** showing the distribution of atomic positions for only those unit cells in which the R intermolecular contact consists of interatomic contacts between: (*a*) two NO_2 groups or (*b*) two Cl groups. Red is O; blue is N; green is Cl; black is C. Note how in (*a*) the molecules are significantly tilted. (*c*) A corresponding plot of the distribution of interatomic distances (deviations from the value in the average structure).

ordered arrangement that does not require such large local strain. In order to confirm the efficacy of these experimental results and in order to try to understand the intermolcular interactions in more detail, we have commenced a study using *ab initio* calculations (Thomas, 2007).

The result is important in a wider context as it emphasizes that local geometry in a crystal can be substantially different from that given by the *average* crystal structure determined from Bragg scattering. This means that extreme care needs to be taken, for example, when attempts are made to predict crystal structures using interatomic energy calculations. It has been shown (Beasley *et al.*, 2006) that even perfectly normal molecular crystal structures that are nominally *ordered* may contain strongly correlated local displacement patterns which mean that, locally, the intermolecular geometry is not well represented by that of the *average* structure. It seems likely that this is a contributing factor in the general difficulty found to date with using *ab initio* methods to predict the crystal structures of molecules with internal flexibility (Day *et al.*, 2005).

References

Beasley, A. G., Welberry, T. R. & Goossens, D. J. (2006). *Acta Cryst.* A**62**, S79.
Butler, B. D. & Welberry, T. R. (1992). *J. Appl. Cryst.* **25**, 391–399.
Cole, J. M., McIntyre, G. J., Thomas, L. H. & Wilson, C. C. (2007). *Acta Cryst.* Submitted for publication.
Cole, J. M., Wilson, C. C., Howard, J. A. K. & Cruickshank, F. R. (2000). *Acta Cryst.* B**56**, 1085–1093.
Correria, N. T., Ramos, J. J. M. & Diogo, H. P. (2002). *J. Phys. Chem. Solids*, **63**, 1717–1722.
Day, G. M. *et al.* (2005). *Acta Cryst.* B**61**, 511–527.
Estermann, M. & Steurer, W. (1998). *Phase Transit.* **67**, 165–195.
Gavezzotti, A. & Simonetta, M. (1975). *Acta Cryst.* A**31**, 645–654.
Goossens, D. J., Welberry, T. R., Heedegen, A. P. & Edwards, A. J. (2005). *Z. Kristallogr.* **222**, 1035–1042.
Hall, P. G. & Horsfall, G. S. (1973). *J. Chem. Soc. Faraday II*, **69**, 1071–1077.
Hehre, W. J., Radom, L., Schleyer, P. R. & Pople, J. (1986). *Ab Initio Molecular Orbital Theory.* New York: John Wiley.
Keen, D. A., Gutmann, M. J. & Wilson, C. C. (2006). *J. Appl. Cryst.* **39**, 714–722.

Khotsyanova, T. L., Babushkina, T. A., Kuznetsova, S. I. & Semin, G. K. (1969). *Zh. Strukt. Khim.* **10**, 525–529.

Kolodziej, H. A., Freundlich, P., Sorriso, S. & Sorriso, C. (1999). *Chem. Phys. Lett.* **305**, 375–380.

Metropolis, N., Rosenbluth, A. W., Rosenbluth, M. N., Teller, A. H. & Teller, E. (1953). *J. Chem. Phys.* **21**, 1087–1092.

Sakurai, T. (1962). *Acta Cryst.* **15**, 1164–1173.

Shahin, M. & Murthy, S. S. N. (2003). *J. Chem. Phys.* **118**, 7495–7503.

Tanaka, I., Iwasaki, F. & Aihara, A. (1974). *Acta Cryst.* **B30**, 1546–1549.

Thomas, L. H. (2007). Ph.D. Thesis. University of Cambridge, UK.

Welberry, T. R. (2001). *Acta Cryst.* A**57**, 244–255.

Welberry, T. R. (2004). *Diffuse X-ray Scattering and Models of Disorder*. IUCr Monographs on Crystallogrphy. Oxford University Press.

Welberry, T. R., Goossens, D. J., Edwards, A. J. & David, W. I. F. (2001). *Acta Cryst.* A**57**, 101–109.

Welberry, T. R., Goossens, D. J., Heerdegen, A. P. & Lee, P. L. (2005). *Z Kristallogr.* **222**, 1052–1058.